Modularized, Reconfigurable and Bidirectional Charging Infrastructure for Electric Vehicles with Silicon Carbide Power Electronics (MoReSiC)

D 4.2 (Month 21)

Title: "The prototype of the full system consisting of the AC-DC bidirectional converter and DSP-based controller tested in both operation modes (active rectifier or inverter) and up to full power range"

Authors: Michał Harasimczuk, Rafał Miśkiewicz, Rafał Kopacz, Jacek Rąbkowski,
Warsaw University of Technology
Radosław Sobieski, Markel

December 2022

Executive summary

The deliverable includes the complete design of the 20 kVA AC/DC converter, which is an input stage of the EV charging station. It was performed by the team from Warsaw University of Technology with support from Markel in terms of mechanical design. Deliverable contains an extension task T4.6 DSP-based controller, which was also included in deliverable D4.1. The most important components of the control board, enabling measurement, control, and communication of the ANPC converter, are described. After that, and an assembly of the control board assembled with the other parts of the ANPC converter, a control algorithm was translated to DSP code and initial experimental results were made. After the initial experimental results, converter was tested under nominal condition of 20 kVA power in both modes: inverter and rectifier.

Table of Contents

1. *DSP-based controller*

In task T4.6 (DSP-based controller), a control board with DSP-based controller TMS320F28388D has been developed for project purposes. The selected DSP device designed for power electronics, including control and measurement for high switching frequency converters. The most important features of the processor are:

- ✓ high 200 MHz core frequency,
- ✓ two CPU,
- ✓ double-precision floating point unit and trigonometric math unit which improve calculation process in our control loop, especially calculate Clark-Park transformation,
- ✓ 512KB of flash on each CPU,
- ✓ controller Area Network (CAN),
- ✓ fours ample-and-hold analog-to-digital converters with 16-bit resolution and high sampling frequency 11 MSPS,
- ✓ 32 Pulse Width Modulator (PWM) channels with dead-time support.

The simplified schematic of the control board based on the selected DSP is shown in Fig. 1. The control board has been designed regarding to task T4.5 to enable all functions described in this task. The power submodule described in WP2 is controlled by the DSP via SN74LVC8T245 non-inverting bus transceiver. That transceiver, in addition to buffering the control signal, also changes the voltage of the logic signal from (0 - 3,3) V on DSP side to (0 - 5) V on the power submodule side. A UCC21750 gate driver was used, providing desaturation protection handling, which makes it possible to stop the control of MOSFETs in fault high current condition, SN74LVCT245 transceiver participates the in transition of MOSFET desaturation (desat) protection signals. In the control board, 8 bus transceivers are used, which are responsible for transmitting the signals for the 18 transistors and their desat protection.

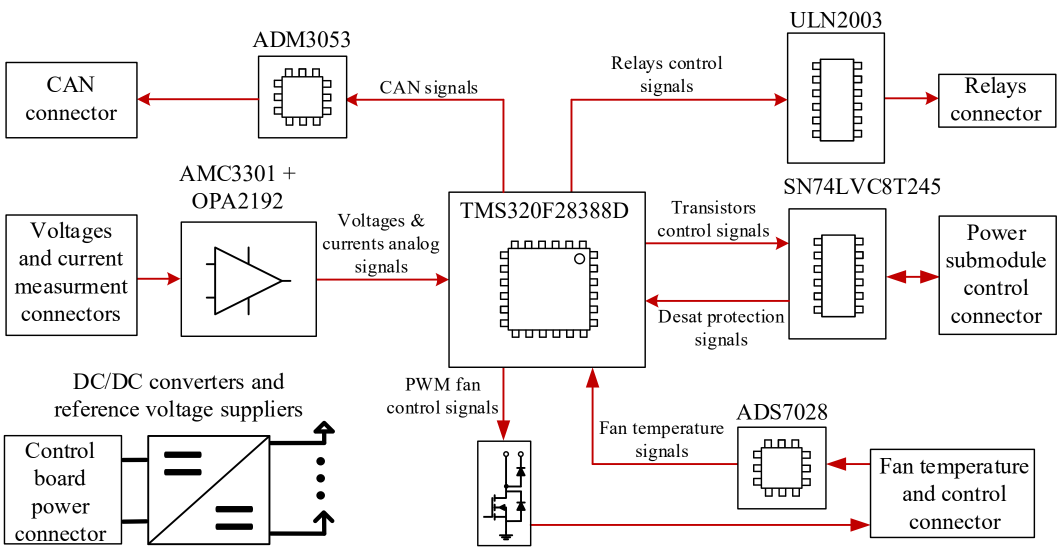

Fig. 1 Simplified schematic of the control board

ULN2003 is a chip with bipolar npn transistor connected in Darlington array. Darlington connection of the npn transistor increases its maximum collector-emitter current, which enables the control via this circuit of relays (in ANPC the are three different relays used, for enabling: AC grid, precharging circuit, and realize connection of high-voltage capacitor with the common dc-link). Besides, ULN2003 consists an internal diode, which reduces the voltage spikes across the transistors during closing relays. To realize communication of the ANPC with other converters, and with the external control computer, a differential CAN interface bus was used. To improve the safety and stability of the ANPC and other components of the system, ADM3053 CAN bus transceiver was used, which realize galvanic isolation between the ANPC control board and other control boards of the system. Moreover, the transceiver consist of an integrated DC/DC converter to supply its secondary side.

A very important part of the system is the proper design of the voltage and current measurements circuits. In the converter, five voltages and five currents (three grid and two dc-link measurements) are monitored. To adjust the measurements to useful voltage signal, LEM current sensors are used to measure the currents, and a resistive divider is used to translate the levels of the measured voltages. That sensors an ad divider were placed on the power board (task T4.3). Next, voltage measurement signals are amplified ten times by AMC3301 inverting amplifier. That component enables isolation between the power and control boards. The output voltages of the AMC3301 are adjusted to the reference voltage of the DSP analog-to-digital converter by using amplifiers based on OPA2192. Measurements are made by DSP 16-bit internal analog-to-digital converter. It is assumed that the voltage and current measurements are performed once every two periods of the converter operation, i.e., every 32 kHz. A measurement should be made fast, to enable the operation of the main program loop once every 32 kHz. Therefore, to relieve the DSP analog-to-digital converters, to measure heat sinks temperature, external analog-to-digital converter chip ADS7028 are used via SPI interface. Heat sink fans are controlled with PWM signal using additional low power MOSFETs and diodes. The control board is powered by external 24 V source with galvanic isolation. Next, that voltage is converted by impulse and linear technique to the control board usable level voltage (+15/-15 V for supplying LEM current sensor, +5/-5 V for supplying measurement amplifiers, separate +5V logic supply, 1.2 V and 3.3 V to power DSP, 3V to power reference source of DSP analog-to-digital converters).

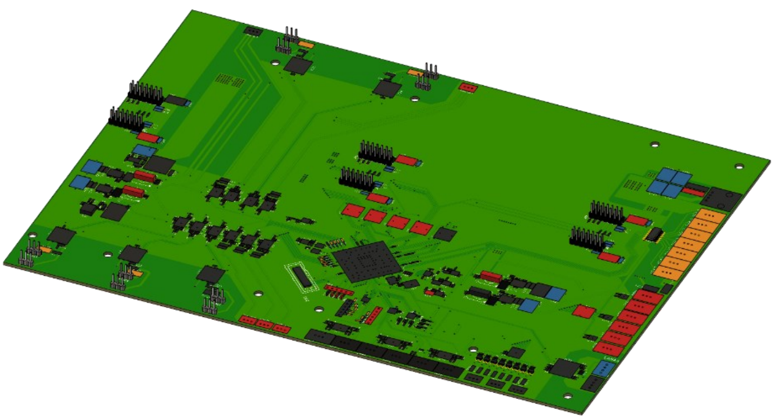

Fig. 2 Model of the control board.

The control board are designed in Cadsoft eagle software as shown above. The model of the control board is depicted in Fig. 2. Dimensions of the control board are 31,5 cm x 23,3 cm, which also allows the board to be placed above the other parts of the system, so that all its parts form a cohesive whole. Fig. 3 shows 3D model of ANPC converter with control board.

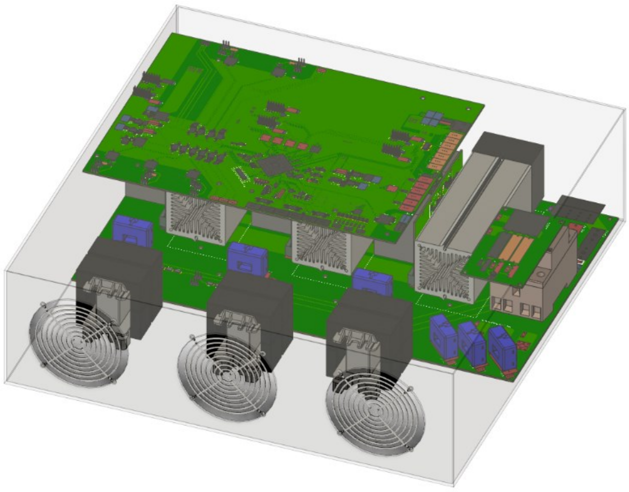

Fig. 3 The 3D model of the 20 kVA AC/DC converter with the control board.

2. *Assembling & initial tests of the AC-DC*

After completing tasks 2, 3, 6 and frame WP2, all the components needed to build the converter have been constructed. Under this task, the ANPC converter was assembled and initial tests confirming the correct performance of previous tasks have been carried out. Fig. 4 shows the prototype of the ANPC converter. Tab. 2 shows the selected parameters of the built AC-DC converter. After that, the measurements were calibrated. Besides, under this task, the converter was assembled and enclosed in 3U rack case (133 mm x 428 mm x 450 mm). More details on the 20 kVA AC/DC converter prototype are provided in description of deliverable D4.2.

Initial tests were conducted in inverter mode under star connected RL load, and in an open-loop system. The modulator operation and measurements of grid and voltages were tested and validated. The converter was tested for safe and stable operation at 1.2 kV dc voltage and 5.4 kW of the output power.

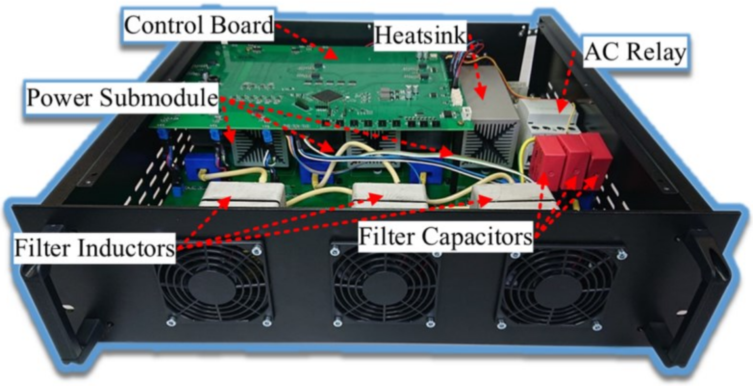

Fig. 4 Prototype of the ANPC converter

Tab. 1 Parameters of the build AC-DC converter

AC side parameters	3 x 230 VAC, 50Hz
Output voltage	1.5 kV DC
Switching frequency	62.5 kHz
Filter inductors	3 x 330 µH
Filter capacitors	3 x 4.7 µF
DC-link capacitors	6 x 60 µF
Power transistors	18 x NTH4L040N120SC1
Nominal output power	20 kW

Fig. 5 shows waveforms obtained in an initial experiment. The obtained shapes of the voltages and currents are in line with theoretical assumptions. This confirms that the parts of the system have been connected correctly and that the modulator and transistors control circuits work properly.

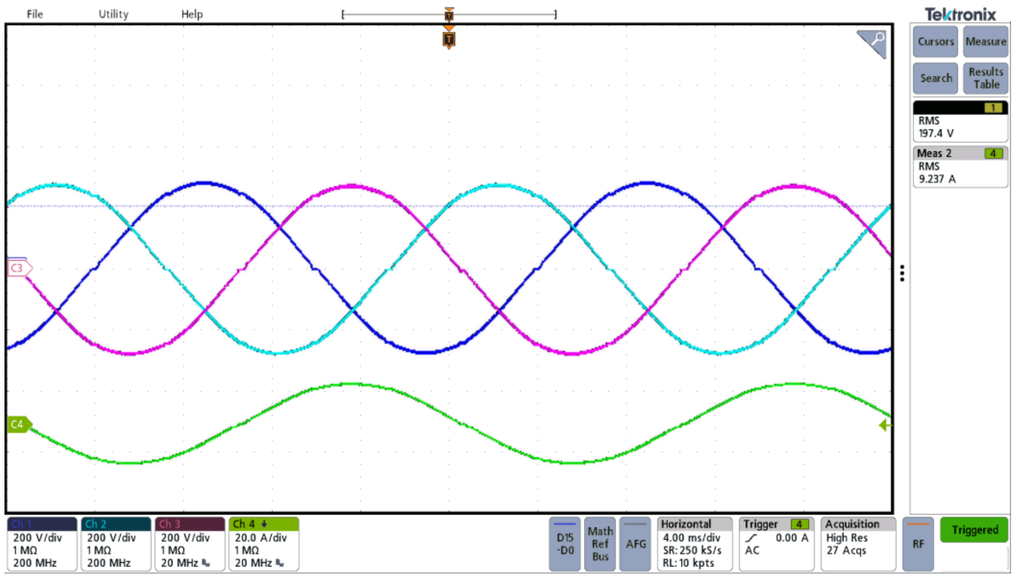

Fig. 5 Initial test on the RL load

3. *Laboratory measurements of the AC-DC converter*

Under this task laboratory measurements of the built converter was carried out in both operation modes: active rectifier and inverter. In order to test the converter at Warsaw University of Technology, the team conducted research using power analyzer PW3390, DC voltage supply/load EA PSB12000-40, a resistive load and digital oscilloscope Tektronix MDO34. In both tested modes the ANPC converter was connected to the grid. Fig. 6 shows the simplified schematic of the ANPC converter. Connection of the ANPC converter to the grid is carried out using an AC relay, to the load it is carried out with a DC relay. Besides, the converter consist of a precharging circuit with three-phase diode rectifier and three resistors. That circuit allows to charge the ANPC dc-link capacitors to line-to-line voltage. That circuit is necessary to enable the AC-relay without a high value of dc-link capacitor charging current.

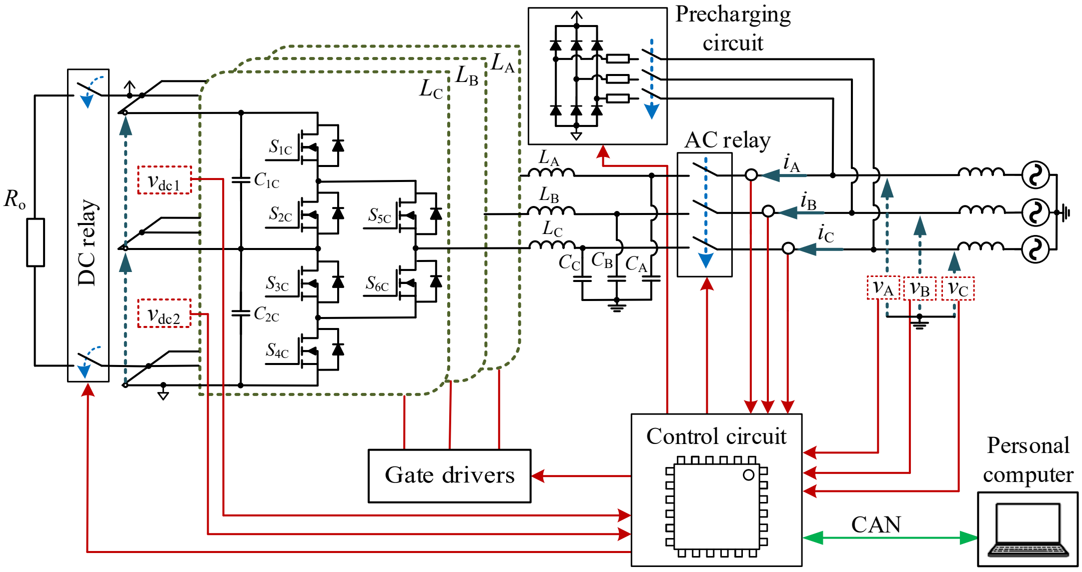

Fig. 6 Schematic of the ANPC converter

The ANPC is controlled using a control circuit block, which has been described in task 5. Moreover, the control circuit is connected to the microcomputer Raspberry Pi via CAN interface in order to turn on/off converter and determine its operating parameters. Fig. 7 and Fig. 8 show waveforms of the tested ANPC converter under turning-on process with two different resistive loads: 240 Ω (Fig. 7) and 120 Ω (Fig. 8). In the Figures, the characteristic intervals in the turning-on process, according with description in task 6, were marked.

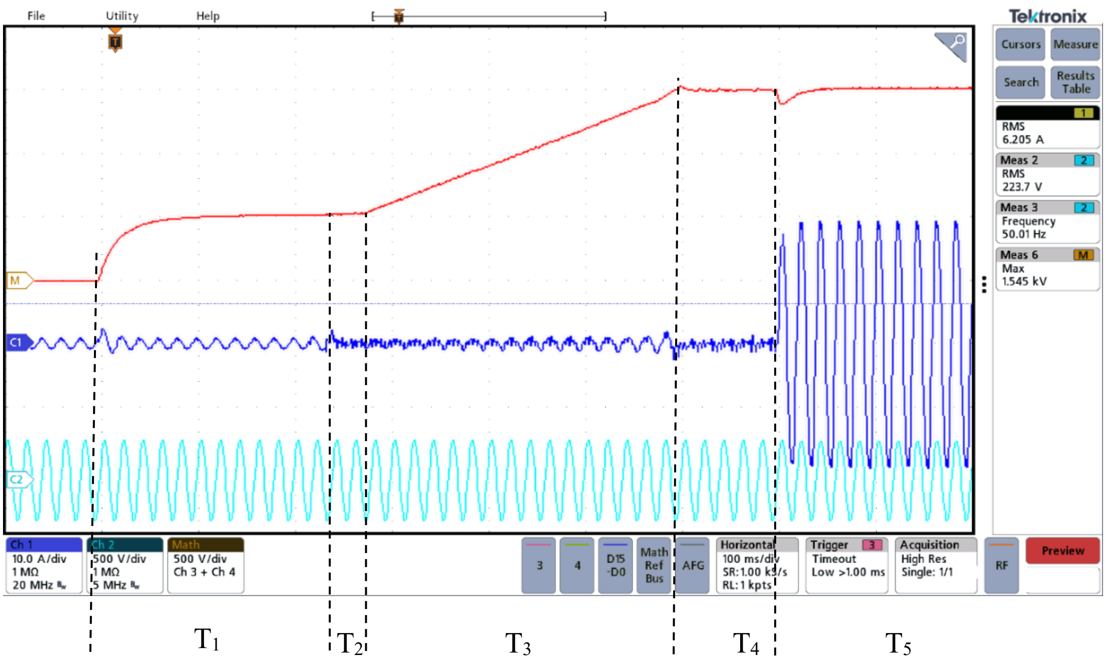

Fig. 7 Exemplary waveforms of the start-up process of the grid converter with enabling 9.4 kW load.

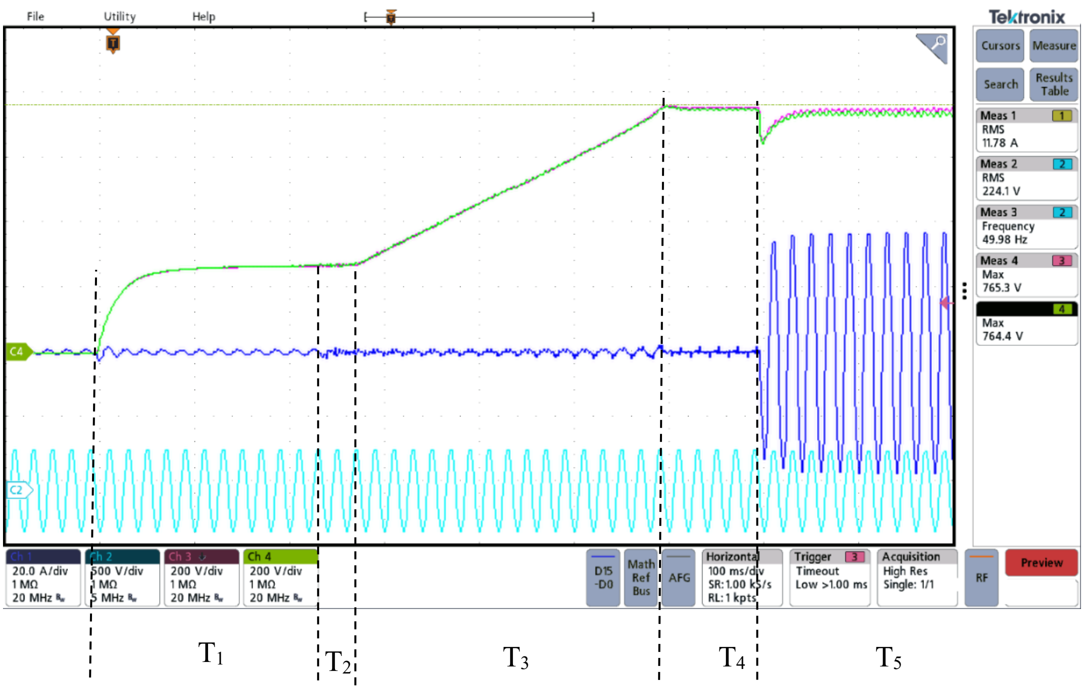

Fig. 8 Exemplary waveforms of the start-up process of the grid converter with enabling 18.8 kW load.

In Fig. 7 and Fig. 8 the waveforms of the dc-link voltage (red), one phase current (blue), one phase voltage (azure), dc-link capacitors voltages (pink and green) are shown. As can be seen from the figures, it takes 600 ms from switching-on the converter (switching on the precharging circuit at the beginning of interval T_1) until it reaches nominal voltage 1.5 kV (beginning of interval T_4). In Fig. 7, at the beginning of interval T_5, a resistive load of 240 Ω is enabled, at a voltage of 1.5 kV, a power of around 9.4 kW is dissipated on this resistance. After enabling such resistance, the voltage dip of around 110 V appeared on the dc-link capacitors. Similarly, the 120 Ω load (Fig. 8) corresponds to the power of around 18.8 kW, and the voltage dip of around 200 V is visible in this case.

Fig. 9 and Fig. 10 show waveforms of grid connected ANPC converter under active rectifier and inverter modes with 1.5 kV dc-link voltage and for different output powers. Figures show waveforms of one phase current (blue), one phase voltage (azure) and dc-link capacitors voltages (pink and green). In both modes the research was carried out with using DC voltage supply/load EA PSB-12000-40. In rectifier mode EA PSB-12000-40 was working as a voltage source, in inverter mode EA PSB-12000-40 was working as a resistive (active) load. In both modes the ripples across $v_{dc1} + v_{dc2}$ voltage are negligibly low. However, the third harmonic ripple of the fundamental frequency between v_{dc1} and v_{dc2} voltages is visible, but it does not exceed 30 V. These ripples grow with increasing output power. The phase current is characterized by some distortions at zero current crossing, especially for lower output power.

Fig. 11 shows iTHD measured for one phase current for different output powers in both modes: inverter and active rectifier. For low output power, iTHD is higher than 10%. However, at nominal output power, the measured iTHD are below required 5% and is around 2% in both modes.

In Fig. 12 the efficiency of the built converter in both modes for various output power is presented. The highest efficiency 97.3%, was measured for 13.3 kW output power under active rectifier mode, and 97.2% in inverter mode for 13 kVA of output power. For nominal conditions the efficiency was the same for both modes and was equal to 97%. The shapes and values of efficiency curves for both modes are similar.

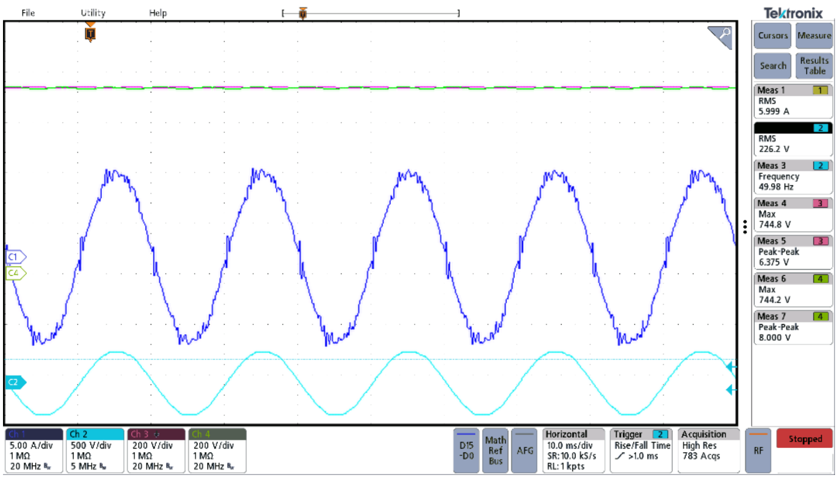

(a)

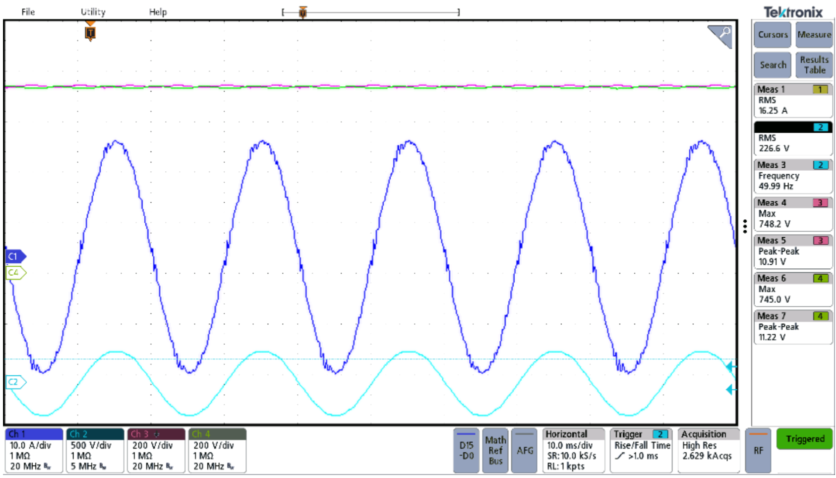

(b)

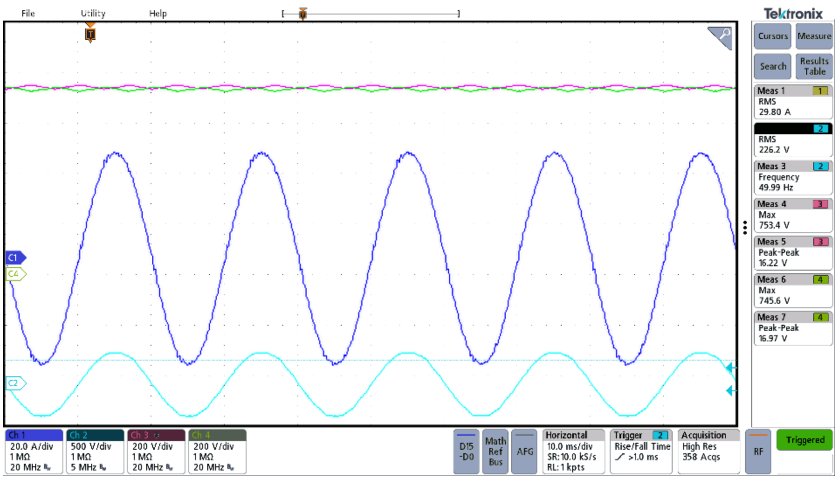

(c)

Fig. 9 Waveforms of the ANPC converter under active rectifier mode, dc-link voltage 1.5 kV and different output power: a) 4.1 kW, b) 11 kW c) 20 kW

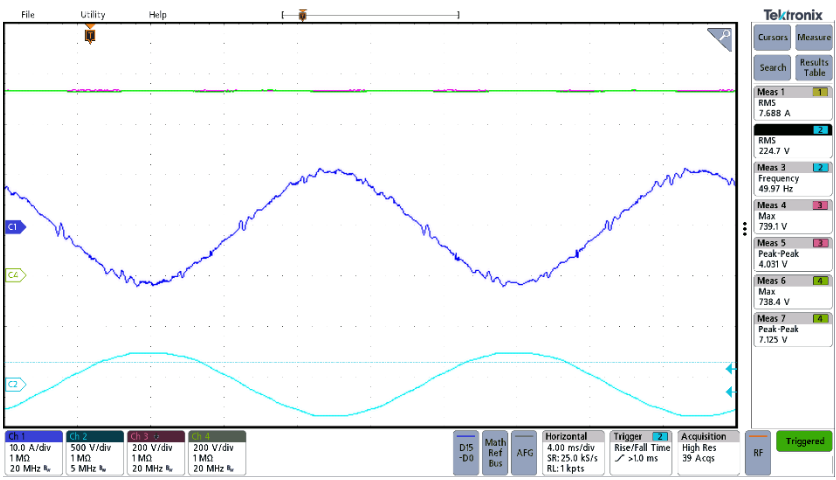

(a)

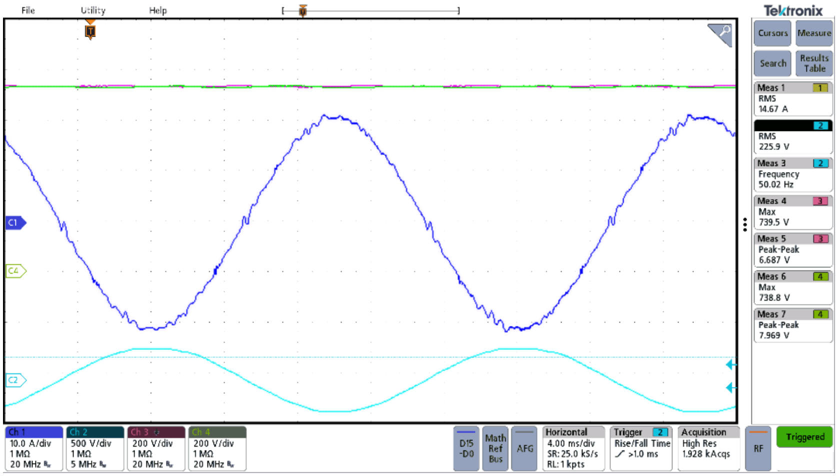

(b)

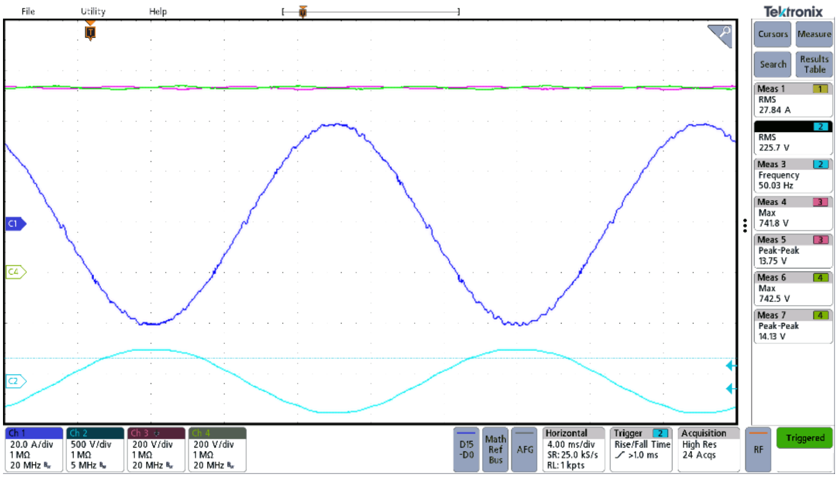

(c)

Fig. 10 Waveforms of the ANPC converter under inverter mode, dc-link voltage 1.5 kV and different output power: a) 5.5 kVA, b) 10.5 kVA c) 20 kVA

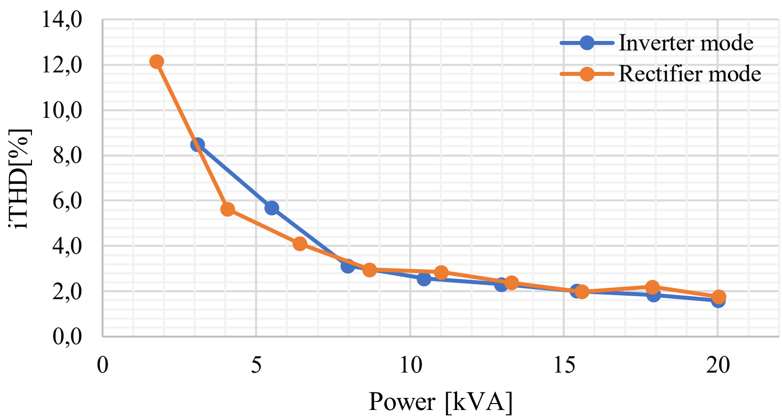

Fig. 11 iTHD of input phase current for different load in active rectifier and inverter mode.

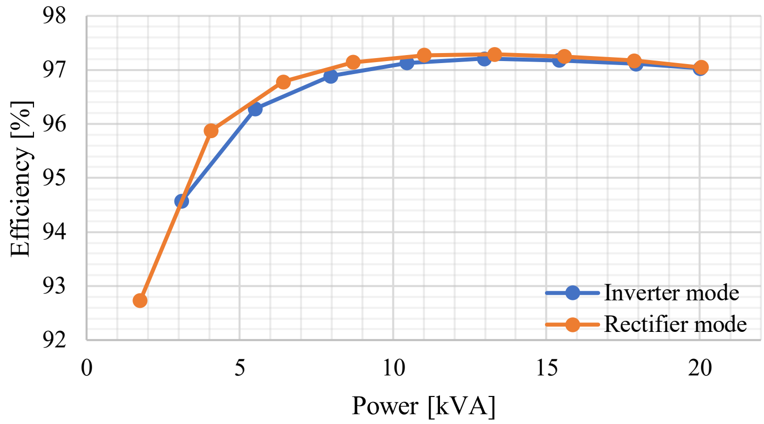

Fig. 12 Efficiency of the ANPC converter

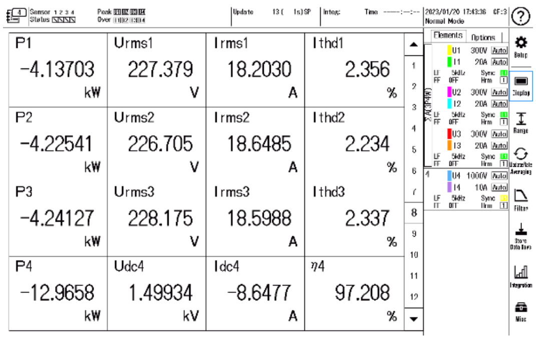

(a)

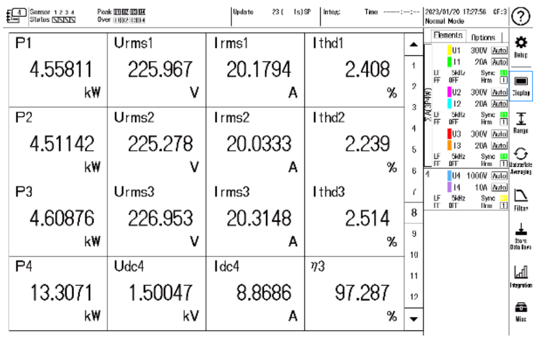

(c)

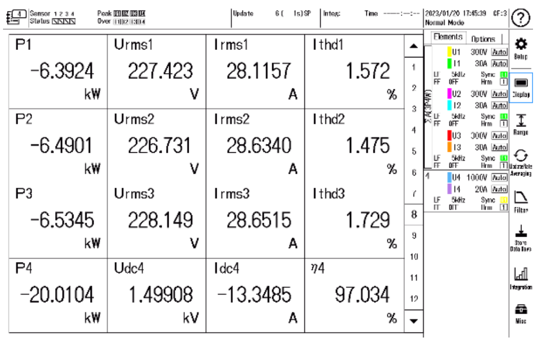

(b)

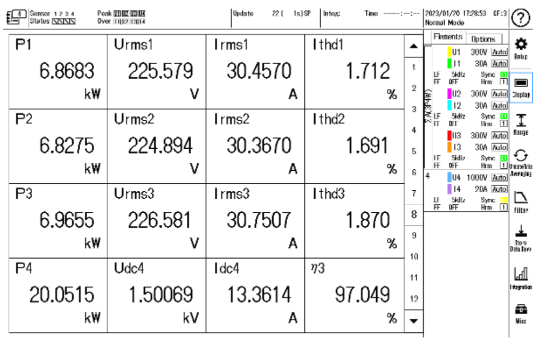

(d)

Fig. 13 Power conversion parameters obtained by using power analyzer when a) and b) is for inverter mode, c) and d) is for active rectifier mode.

Fig. 13 show power conversion parameters obtained using power analyzer PW3390 where: $P_1 - P_3$ are each phase grid power, P_4 is input power, $U_{rms1} - U_{rms3}$ are rms grid voltages of each phase, U_{dc4} is the dc-link voltage, $I_{rms1} - I_{rms3}$ are rms grid currents of each phase, I_{dc4} is the dc-link current, $I_{thd1} - I_{thd3}$ are current THD of each phase, η_3 – is the power conversion efficiency.

4. Summary

The deliverable D4.2 “The prototype of the full system consisting of the AC-DC bidirectional converter and DSP-based controller tested in both operation modes (active rectifier and inverter) and up to full power range (20 kVA)” have been accomplished with the end of 21st month of the project. Based on a theoretical and simulation study described in deliverable D.4.1, the converter was designed and built (D4.2), then it was subjected to laboratory tests to check the parameters of energy conversion. In both modes: active rectifier, and inverter, the efficiency of 97% was achieved for nominal conditions (dc-link voltage: +750/0/-750 V and power 20 kVA). Unfortunately, due to relatively high DC link voltage and operation at a low modulation index, it was not possible to achieve expected efficiency 98%, however, in the full scale system rated at hundreds of kWs and higher grid voltage, in our opinion it is perfectly possible. Performed tests show current quality in both modes at nominal condition are below 2%, well below required 5%. In summary, all declared parameters of the ANPC converter under WP4 were achieved, except the efficiency above 98%.